

# Effects of momentum-dependent symmetry potential on heavy-ion collisions induced by neutron-rich nuclei

Bao-An Li<sup>a</sup>, Champak B. Das<sup>b\*</sup>, Subal Das Gupta<sup>b</sup> and Charles Gale<sup>b</sup>

<sup>a</sup>*Department of Chemistry and Physics*

*P.O. Box 419, Arkansas State University*

*State University, Arkansas 72467-0419, USA*

<sup>b</sup>*Physics Department, McGill University, Montréal, Canada H3A 2T8*

(November 16, 2018)

## Abstract

Using an isospin- and momentum-dependent transport model we study effects of the momentum-dependent symmetry potential on heavy-ion collisions induced by neutron-rich nuclei. It is found that symmetry potentials with and without the momentum-dependence but corresponding to the same density-dependent symmetry energy  $E_{sym}(\rho)$  lead to significantly different predictions on several  $E_{sym}(\rho)$ -sensitive experimental observables especially for energetic nucleons. The momentum- and density-dependence of the symmetry potential have to be determined simultaneously in order to extract the  $E_{sym}(\rho)$  accurately. The isospin asymmetry of midrapidity nucleons at high transverse momenta is particularly sensitive to the momentum-dependence of the symmetry potential. It is thus very useful for investigating accurately the

---

\*Present address: Variable Energy Cyclotron Center, 1/AF, Bidhannagar, Kolkata-700 064, India

equation of state of dense neutron-rich matter.  
25.70.-z, 25.70.Pq., 24.10.Lx

## I. INTRODUCTION

The equation of state (EOS) of asymmetric nuclear matter at density  $\rho$  and isospin asymmetry  $\delta \equiv (\rho_n - \rho_p)/(\rho_p + \rho_n)$  is usually expressed as

$$E(\rho, \delta) = E(\rho, \delta = 0) + E_{\text{sym}}(\rho)\delta^2 + \mathcal{O}(\delta^4), \quad (1)$$

where  $E_{\text{sym}}(\rho)$  is the nuclear symmetry energy. The latter is very important for many interesting astrophysical problems and yet poorly known for dense neutron-rich matter [1–3]. Predictions based on various many-body theories diverge widely, especially at high densities. In fact, even the sign of the symmetry energy above  $3\rho_0$  is still very uncertain [4]. Since nuclear reactions induced by high energy radioactive beams can produce transiently dense neutron-rich matter, the planned Rare Isotope Accelerator (RIA) and the new accelerator facility at GSI provide the first opportunity in terrestrial laboratories to explore experimentally the EOS of dense neutron-rich matter [5–8]. Crucial to the extraction of critical information about the  $E_{\text{sym}}(\rho)$  is the comparison between experimental data and transport model calculations. Based on isospin-dependent transport model calculations, several experimental observables have been identified as promising probes of the  $E_{\text{sym}}(\rho)$ , such as, the neutron/proton ratio [9], isoscaling in nuclear multifragmentation [10–13], the neutron-proton differential flow [14–16], the neutron-proton correlation function [17] and the isobaric yield ratios of light clusters [18].

An important input to the transport models are the isovector (symmetry) and isoscalar potentials. However, in all transport models for heavy-ion collisions the momentum-dependence of the symmetry potential was seldom taken into account. In the recent work of ref. [19] effects of the neutron-proton effective mass splitting due to the momentum-dependent nuclear potentials were studied using Bombaci’s parameterization of single nucleon potential [4]. Nevertheless, effects of the momentum-dependence of the symmetry potential in heavy-ion collisions are still largely unknown. On the other hand, effects of the momentum-dependence of the isoscalar potential in nuclear reactions are well-known [20–26].

This is mainly because only very recently was the momentum-dependence of the symmetry potential given in a form practically usable in transport model calculations [27]. In this work, we study in detail effects of the momentum-dependence of the symmetry potential on heavy-ion collisions induced by neutron-rich nuclei. A short report of this study can be found in ref. [28]. In the next section, we discuss the momentum-dependence of the symmetry potential using as a guide results of Hartree-Fock calculations with Gogny effective interactions. The strengths of the symmetry potential with and without the momentum-dependence are compared. In section III, we present and discuss effects of the momentum-dependence of the symmetry potential on several experimental observables in heavy-ion collisions induced by neutron-rich nuclei. A summary is given at the end.

## II. MOMENTUM-DEPENDENCE OF THE SYMMETRY POTENTIAL

That the momentum-dependence of the single particle potential is different for neutrons and protons in asymmetric nuclear matter is well-known and has been a subject of intensive research based on various many-body theories using non-local interactions, see e.g., ref. [4] for a review. Experimentally, it is known that the strength of nuclear symmetry potential decreases linearly from about  $28 \pm 6$  MeV with increasing kinetic energy with a slope of about 0.1-0.2 from optical model analyses of nucleon-nucleus scattering data [29]. However, the available data is limited only to nucleon energies less than 100 MeV. Guided by a Hartree-Fock calculation using the Gogny effective interaction, the single nucleon potential was recently parameterized as [27]

$$\begin{aligned}
U(\rho, \delta, \vec{p}, \tau) = & A_u \frac{\rho_{\tau'}}{\rho_0} + A_l \frac{\rho_{\tau}}{\rho_0} \\
& + B \left( \frac{\rho}{\rho_0} \right)^{\sigma} (1 - x \delta^2) - 8\tau x \frac{B}{\sigma + 1} \frac{\rho^{\sigma-1}}{\rho_0^{\sigma}} \delta \rho_{\tau'} \\
& + \frac{2C_{\tau, \tau}}{\rho_0} \int d^3 p' \frac{f_{\tau}(\vec{r}, \vec{p}')}{1 + (\vec{p} - \vec{p}')^2 / \Lambda^2} \\
& + \frac{2C_{\tau, \tau'}}{\rho_0} \int d^3 p' \frac{f_{\tau'}(\vec{r}, \vec{p}')}{1 + (\vec{p} - \vec{p}')^2 / \Lambda^2}
\end{aligned} \tag{2}$$

The parameter  $x$  can be adjusted to mimic predictions on the density dependence of the symmetry energy  $E_{sym}(\rho)$  by microscopic and/or phenomenological many-body theories. In the above  $\tau = 1/2$  ( $-1/2$ ) for neutrons (protons) and  $\tau \neq \tau'$ ;  $\sigma = 4/3$ ;  $f_\tau(\vec{r}, \vec{p})$  is the phase space distribution function at coordinate  $\vec{r}$  and momentum  $\vec{p}$ . The parameters  $A_u, A_l, B, C_{\tau,\tau}, C_{\tau,\tau'}$  and  $\Lambda$  were obtained by fitting the momentum-dependence of the  $U(\rho, \delta, \vec{p}, \tau)$  predicted by the Gogny Hartree-Fock and/or the Brueckner-Hartree-Fock calculations, saturation properties of symmetric nuclear matter and the symmetry energy of 30 MeV at normal nuclear matter density  $\rho_0 = 0.16/fm^3$  [27]. More specifically,  $B=106.35$  MeV and  $\Lambda = p_F^0$  is the nucleon Fermi momentum in symmetric nuclear matter.  $A_u$  and  $A_l$  depend on the  $x$  parameter according to

$$A_u(x) = -95.98 - x \frac{2B}{\sigma + 1}, \quad (3)$$

$$A_l(x) = -120.57 + x \frac{2B}{\sigma + 1}. \quad (4)$$

The compressibility of symmetric nuclear matter  $K_0$  is set to be 211 MeV.

The momentum-dependence of the symmetry potential stems from the different interaction strength parameters  $C_{\tau,\tau'}$  and  $C_{\tau,\tau}$  for a nucleon of isospin  $\tau$  interacting, respectively, with unlike and like nucleons in the background fields. More specifically, we obtained  $C_{unlike} = -103.4$  MeV and  $C_{like} = -11.7$  MeV. One characteristic of the momentum dependence of the symmetry potential is the different effective masses for neutrons and protons in isospin asymmetric nuclear matter. In terms of the single particle potential  $U(\rho, \delta, \vec{p}, \tau)$  the nucleon effective mass is defined as

$$\frac{m_\tau^*}{m_\tau} = \left[ 1 + \frac{m_\tau}{p} \frac{dU}{dp} \right]_{p_F^\tau}^{-1}. \quad (5)$$

Since the momentum dependent part of the single particle potential in eq. 2 is independent of the parameter  $x$ , the nucleon effective mass is the same for different symmetry energies. Shown in Fig. 1 are the nucleon effective masses as a function of density (upper window) and isospin asymmetry (lower window). These results are consistent with the Brueckner Hartree-Fock predictions [37].

## FIGURES

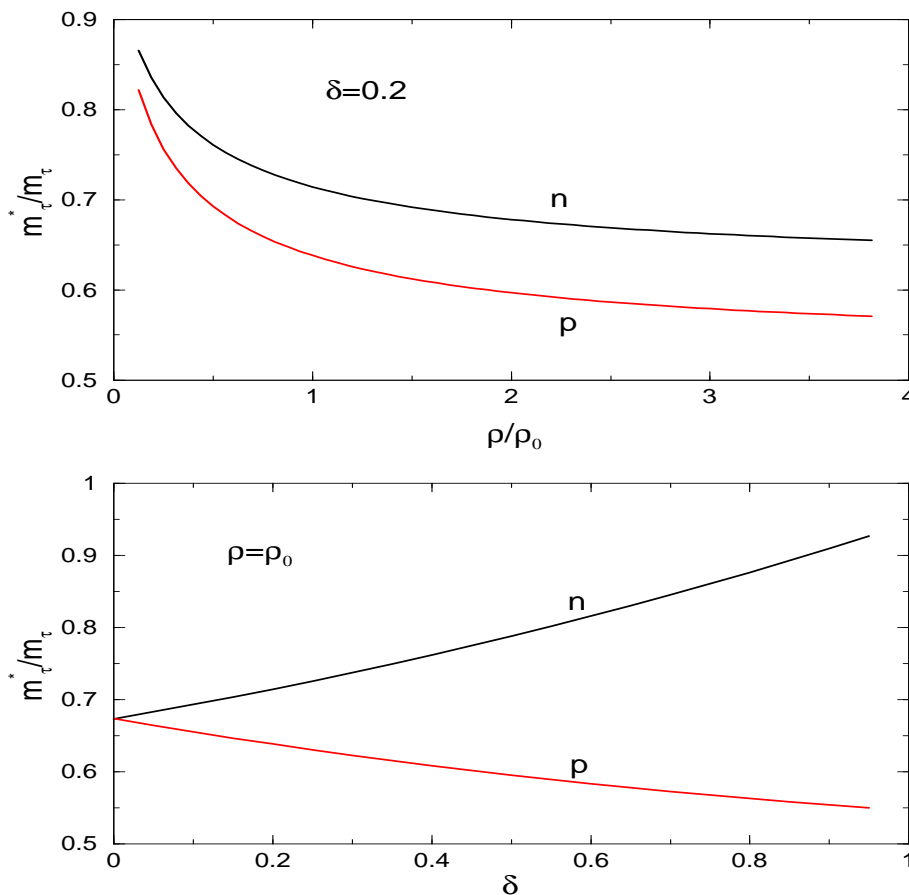


FIG. 1. Nucleon effective masses as a function of density (upper window) and isospin asymmetry (lower window).

The parameter  $x$  was introduced to reflect the largely uncertain behavior of  $E_{sym}(\rho)$  at supranormal densities, specifically its potential part  $E_{sym}^p(\rho)$ . The latter corresponding to  $x = 1$  (denoted by MDI(1) which gives the same  $E_{sym}(\rho)$  as the default Gogny interaction) and  $x = 0$  (MDI(0)) are shown in Fig. 2. For comparisons we have also included the potential part of the more stiffer symmetry energy  $E_{sym}^{RMF}(\rho) \equiv 30\rho/\rho_0$ , predicted by several models, such as, the Relativistic-Mean-Field (RMF) model. As a reference, the kinetic contribution  $E_{sym}^k(\rho) = \hbar^2/6m_n(3\pi^2\rho/2)^{2/3}$  is also shown. The variation of  $E_{sym}(\rho)$  resulted by changing from the MDI(1) to the MDI(0) parameter set is well within the uncertain

range predicted by various many-body theories, see e.g., refs. [32,33,37]. We found that the potential contribution to the symmetry energy can be parameterized as

$$E_{sym}^p(\rho) = 3.08 + 39.6u - 29.2u^2 + 5.68u^3 - 0.523u^4 \quad (6)$$

for the MDI(1) (Gogny) interaction and

$$E_{sym}^p(\rho) = 1.27 + 25.4u - 9.31u^2 + 2.17u^3 - 0.21u^4 \quad (7)$$

for the MDI(0) interaction, where  $u \equiv \rho/\rho_0$  is the reduced nucleon density.

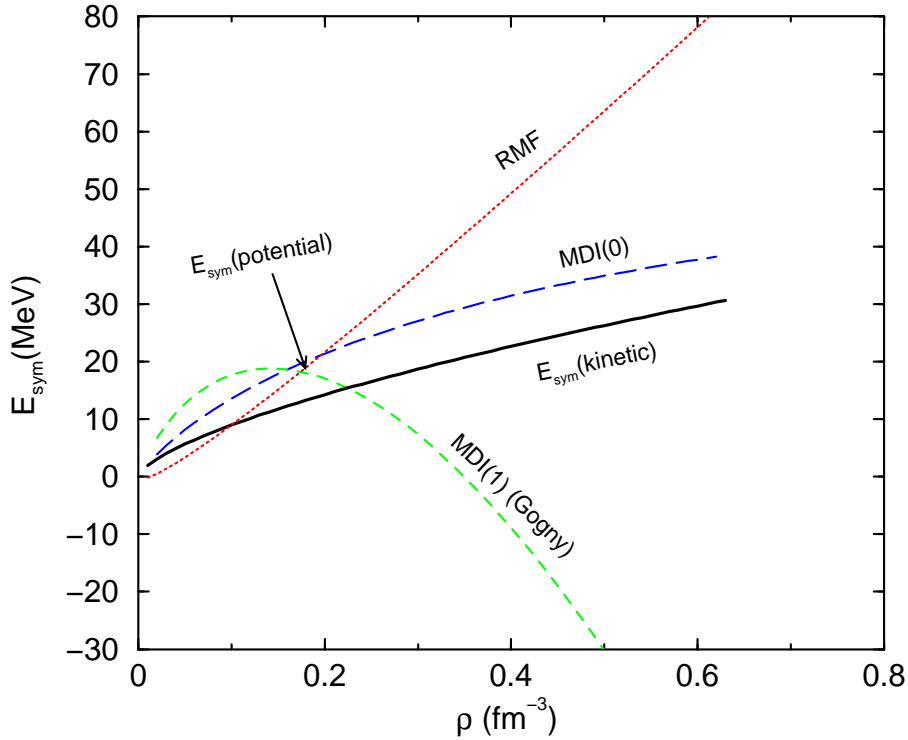


FIG. 2. The density dependence of the potential and kinetic parts of nuclear symmetry energy.

To compare with the experimentally found momentum-dependence of the symmetry potential in nucleon-nucleus scatterings, we illustrate in Fig. 3 the strength of the symmetry potential  $(U_n - U_p)/2\delta$  as a function of nucleon kinetic energy at densities of  $0.5\rho_0$ ,  $\rho_0$  and  $2\rho_0$ , for  $x = 1$  (left) and  $x = 0$  (right), respectively. The results are obtained by using  $\delta = 0.2$ . However, since the isovector part of the nucleon potential is approximately proportional to

$\delta$ , the quantity  $(U_n - U_p)/2\delta$  is approximately independent of  $\delta$ . At normal density, for both  $x = 1$  and  $x = 0$  the strength of symmetry potential decreases from about 33 MeV at  $E_{kin} = 0$  with a slope of about 0.22 for  $E_{kin} \leq 100$  MeV in general agreement with the nucleon-nucleus scattering data. Moreover, it is seen that the strength approaches zero above about 200 MeV. At other densities, however, the predictions are dramatically different for  $x = 1$  and  $x = 0$  especially at high densities. For  $\rho = 2\rho_0$ , for instance, the strength of symmetry potential is negative and decreases quickly with energy indicating a stronger attractive/repulsive symmetry potentials for neutrons/protons with  $x = 1$ . With  $x = 0$ , however, at the same density  $\rho = 2\rho_0$  the strength of the symmetry potential is now positive indicating the repulsive/attractive nature of the symmetry potential for neutrons/protons. It is thus characteristically different from the  $x = 1$  case. It is also seen that the strength of the symmetry potential decreases relatively slowly with  $x = 0$ . These different energy dependences of the symmetry potential are correlated to the negative and positive potential contribution to the symmetry energy at high densities for  $x = 1$  and  $x = 0$ , respectively.

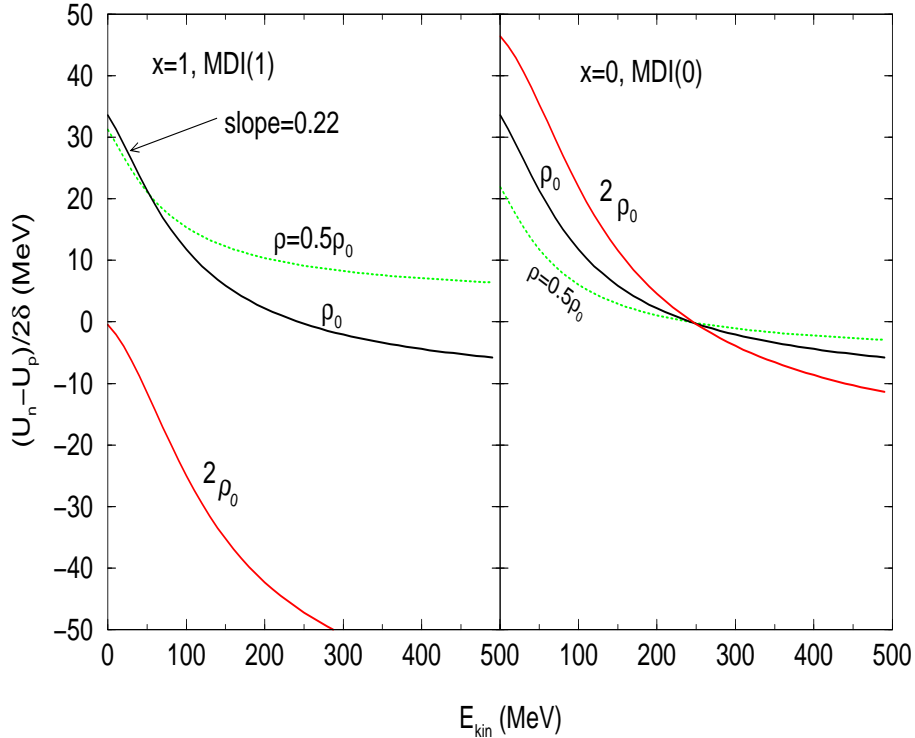




FIG. 3. Strength of the symmetry potential as a function of kinetic energy at three densities for  $x = 1$  (left) and  $x = 0$  (right).

Since the C-terms in the single particle potential depend inseparably on the density, momentum and isospin, to investigate effects of the momentum-dependence of the symmetry potential we shall also compare results obtained using eq. 2 with those obtained using a single nucleon potential  $U_{noms}(\rho, \delta, \vec{p}, \tau) \equiv U_0(\rho, \vec{p}) + U_{sym}(\rho, \delta, \tau)$  that has almost the same momentum-dependent isoscalar part  $U_0(\rho, \vec{p})$  as that embedded in eq. 2 and a momentum-independent symmetry potential  $U_{sym}(\rho, \delta, \tau)$  that gives the same  $E_{sym}(\rho)$  as eq. 2. The momentum-independent  $U_{sym}(\rho, \delta, \tau)$  can be obtained from

$$U_{sym}(\rho, \delta, \tau) = \partial W_{sym} / \partial \rho \tau, \quad (8)$$

where  $W_{sym}$  is the isospin-dependent part of the potential energy density

$$W_{sym} = E_{sym}^p(\rho) \cdot \rho \cdot \delta^2. \quad (9)$$

For the symmetry energy  $E_{sym}^{RMF}(\rho)$ , for instance, one obtains

$$U_{sym}^{RMF}(\rho, \delta, \tau) = 4\tau\delta(30u - 12.7u^{2/3}) + 4.23u^{2/3}\delta^2. \quad (10)$$

Using the parameterizations for  $E_{sym}^p(\rho)$  in eqs. 6 and 7, we obtain

$$\begin{aligned} U_{sym}^{MDI1}(\rho, \delta, \tau) &= 4\tau\delta(3.08 + 39.6u - 29.2u^2 + 5.68u^3 \\ &- 0.52u^4) - \delta^2(3.08 + 29.2u^2 - 11.4u^3 + 1.57u^4) \end{aligned} \quad (11)$$

for the MDI(1) parameter set and

$$\begin{aligned} U_{sym}^{MDI0}(\rho, \delta, \tau) &= 4\tau\delta(1.27 + 25.4u - 9.31u^2 + 2.17u^3 \\ &- 0.21u^4) - \delta^2(1.27 + 9.31u^2 - 4.33u^3 + 0.63u^4) \end{aligned} \quad (12)$$

for the MDI(0) parameter set. The momentum-dependent isoscalar potential  $U_0(\rho, \vec{p})$  will be given in the following shortly.

The strengths of the symmetry potentials with and without the momentum-dependence but corresponding to the same  $E_{sym}(\rho)$  are compared in Fig. 4 by examining the difference between neutron and proton potentials  $(U_n - U_p)/2\delta$ . Again, this quantity is approximately independent of the parameter  $\delta$ . The symmetry potential without the momentum-dependence is higher in magnitude and has generally steeper slopes than the momentum-dependent one for  $\rho/\rho_0 \leq 2.3$  with the MDI(1) parameter set and at all densities for the MDI(0) parameter set. Moreover, the strength of momentum-dependent symmetry potentials decreases with the increasing momentum. Thus the difference between the symmetry potentials with and without the momentum-dependence is larger for nucleons with higher momenta.

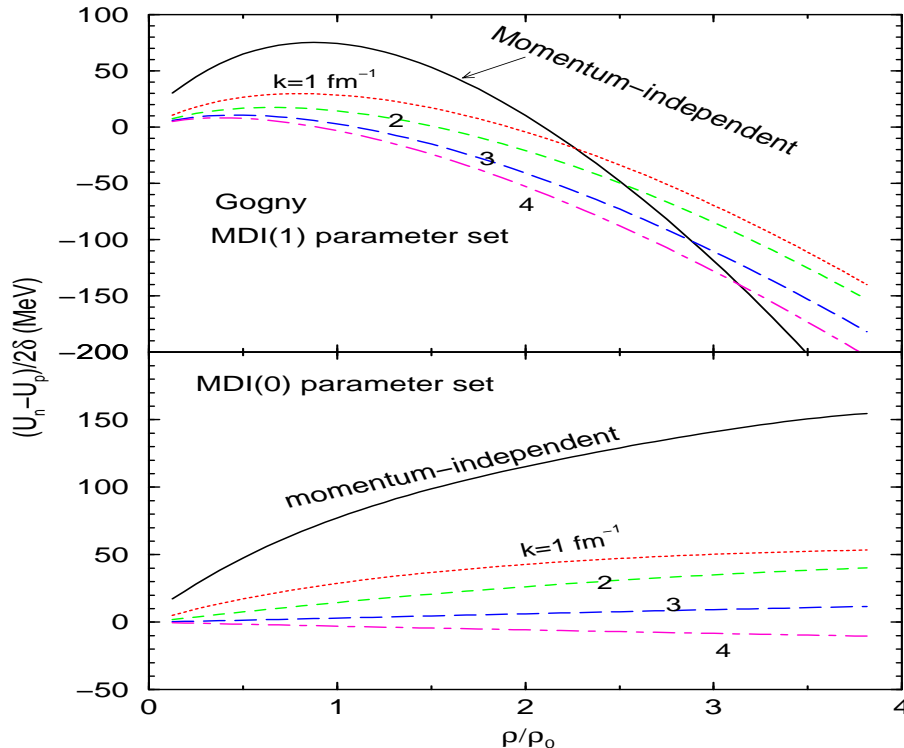


FIG. 4. Strengths of the symmetry potentials with and without (solid) the momentum-dependence as a function of density as measured by the difference between neutron and proton potentials.

To identify reliably effects of the momentum-dependence of the symmetry potential with-

out much interference from density effects the  $U_{noms}(\rho, \delta, \vec{p}, \tau)$  should lead to about the same reaction dynamics and evolution of density profiles as the single particle potential in eq. 2. Both of them are mainly determined by the isoscalar potential for which we select the original momentum-dependent Yukawa interaction (MDYI) [22]

$$U_0(\rho, \vec{p}) = -110.44u + 140.9u^{1.24} - \frac{130}{\rho_0} \int d^3p' \frac{f(\vec{r}, \vec{p}')}{1 + (\vec{p} - \vec{p}')^2 / (1.58p_F^0)^2}, \quad (13)$$

where  $p_F^0$  is the Fermi momentum. The compressibility  $K_0$  for this interaction is 215 MeV. This potential is compared with the variational calculation using the  $UV14 + UVII$  interactions in Fig. 5. Except at high densities but low momenta the MDYI interaction gives about the same isoscalar potential as the variational approach as first found in ref. [22].

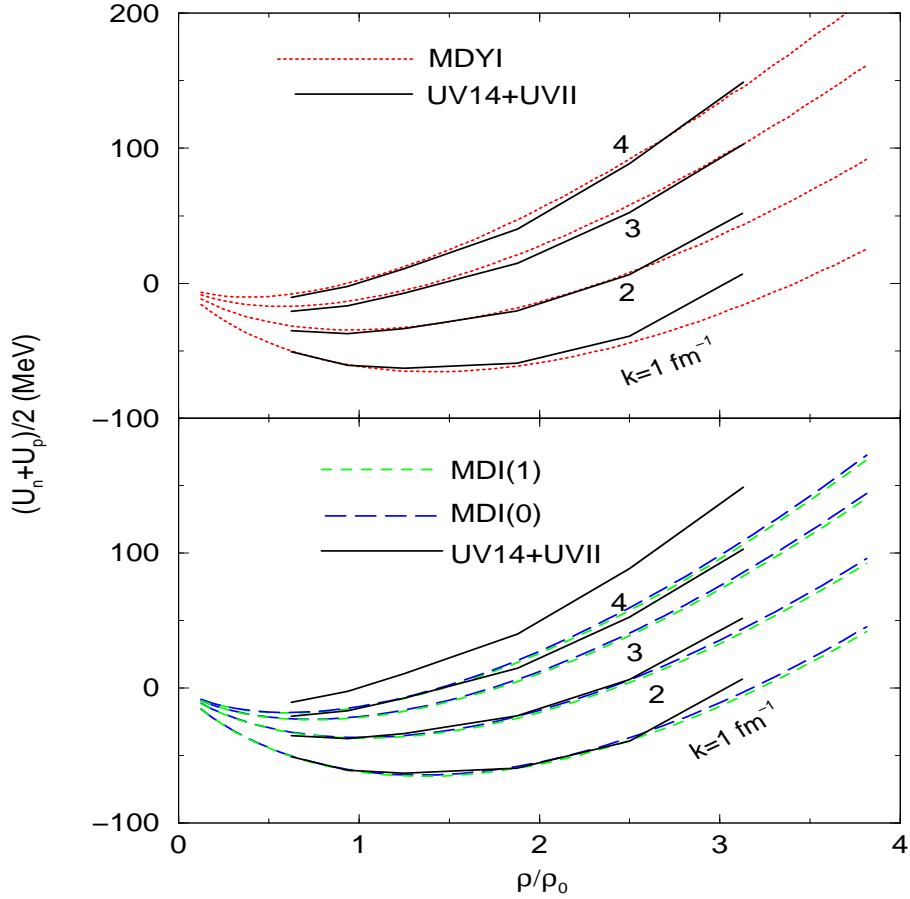


FIG. 5. Strengths of the isoscalar potential as a function of density at the four wave numbers for the MDI(1) and MDI(0) parameter sets (lower window) as well as the MDYI (upper window) interaction in comparison with the variational many-body calculations using the *UV14* two-body and the *UVII* three-body potentials. (upper window)

In the lower window of Fig. 5 we compare the isoscalar part  $(U_n + U_p)/2$  of the single nucleon potentials corresponding to the MDI(1) and MDI(0) parameter sets. It is seen that they have roughly the same values at all wave numbers  $k$  examined, except at high densities where the MDI(0) parameter set leads to slightly stiffer isoscalar potentials. This feature ensures that the differences we see in reaction calculations using the MDI(1) and MDI(0) parameter sets are truly due to the different symmetry potentials. As a reference we have also included Wiringa's calculations of the isoscalar potentials within the variational many-body approach using the *UV14* two-body potential and the *UVII* three-body potential. The single nucleon potential was obtained by using a realistic Hamiltonian that fits nucleon-nucleon scattering data, few-body nuclear binding energies and nuclear matter saturation properties [30]. It was shown that combinations of different two-body and three-body forces lead to slightly different single nucleon potential especially at high densities and/or high momenta. It is seen that for wave numbers less than about  $2fm^{-1}$  the MDI(1) and MDI(0) results are very close to that of the variational calculations. At higher wave numbers, however, the variational results are higher. For our studies of isospin effects in this work isoscalar potentials are less important as long as the reaction dynamics is about right. We thus consider the isoscalar parts of both the MDI(1) and MDI(0) interactions as very reasonable for the purpose of this work.

Overall, the MDYI interaction leads to about the same isoscalar potential as the MDI(1) and MDI(0) interactions for  $k$  less than about  $2fm^{-1}$ . We shall also verify numerically that the potential  $U_{noms}(\rho, \delta, \vec{p}, \tau)$  constructed this way indeed leads to about the same reaction dynamics and the evolution of density profiles as the potential in eq. 2. For comparisons and identify effects due to the momentum-dependence and stiffness of the isoscalar potential, we

use occasionally also the momentum-independent Bertsch-Kruse-DasGupta (BKD) isoscalar potentials. The soft BKD is given by [31]

$$U_0(\rho) = -356u + 303u^{7/6}, \quad (14)$$

and stiff BKD is given by

$$U_0(\rho) = -124u + 70.5u^2. \quad (15)$$

The compressibilities of these two potentials are  $K_0 = 201$  and  $377$  MeV, respectively.

### III. RESULTS AND DISCUSSIONS

In this section we examine effects of the momentum-dependence of the symmetry potential on the reaction dynamics and several experimental observables. Several observables are known to be sensitive only to the symmetry potential but not to the isoscalar potential. They are mainly neutron-proton differential or relative quantities [9,14] where effects of the isoscalar potential with or without the momentum-dependence are largely canceled out. Moreover, these observables are also not sensitive to the in-medium nucleon-nucleon cross sections [9,17,18] since the latter act approximately identically on both neutrons and protons. Assuming the symmetry potential is momentum-independent, these observables were previously proposed as promising probes of the density-dependence of the symmetry energy. Our emphasis in this work will be on searching for experimental observables that can be used to determine simultaneously both the density- and momentum-dependence of the symmetry potential, and thus to determine uniquely the density-dependence of the symmetry energy. These studies are carried out within an isospin-dependent transport model [9], for the latest review of this model we refer the reader to ref. [7]. In this work we concentrate on  $^{132}\text{Sn}+^{124}\text{Sn}$  reactions at the highest RIA beam energy of 400 MeV/nucleon.

### A. Effects on reaction dynamics

Shown in Fig. 6 are the evolutions of central baryon densities in  $^{132}\text{Sn}+^{124}\text{Sn}$  reactions at a beam energy of 400 MeV/nucleon and an impact parameter of 1 fm with various potentials. In the upper window, we first compare results obtained by using the soft BKD (solid thin line) and the MDYI (dot-dashed line) isoscalar potentials but the same symmetry potential  $U_{sym}^{RMF}(\rho)$ . It is seen that the soft BKD leads to a higher compression by about 10% compared to the MDYI interaction in agreement with previous findings in many studies.

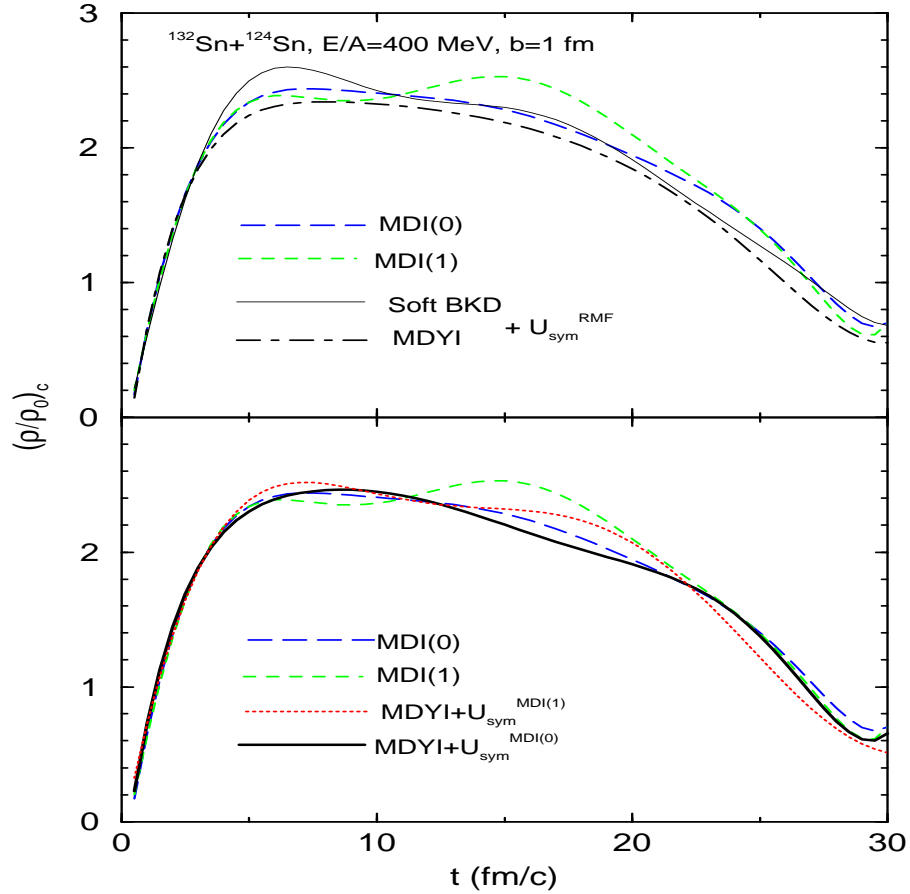


FIG. 6. Evolution of central baryon density with various potentials in the  $^{132}\text{Sn}+^{124}\text{Sn}$  reaction at a beam energy of 400 MeV/nucleon and an impact parameter of 1 fm.

Next, we compare results obtained with the MDI(0) (long dashed line) and the MDI(1)

(dashed line) potentials. As we have discussed earlier they have about the same isoscalar potential while very different symmetry potentials as shown in Fig. 4. It is interesting to notice that starting at about 10 fm/c when the central density is above about  $2.4\rho_0$ , the central density for the MDI(1) starts increasing significantly with respect to the MDI(0) case. This is what we have expected based on eq. 1 and the density dependence of the symmetry energy. The relative values of the central densities reflect closely the relative stiffnesses of the underlying equations of state. The above observation is due to a softening of the underlying EOS in the MDI(1) case. As shown in Fig. 2, the potential part of the symmetry energy increases continuously for the MDI(0) while decreases with increasing density above  $\rho_0$  for the MDI(1) case. In fact, starting at about  $2.4\rho_0$ , the symmetry energy becomes negative with the MDI(1) parameter set, leading thus to the more compressed central region. Overall, however, the differences in central densities using different potentials are less than about 10%.

In the lower window of Fig. 6, we study effects of the momentum-dependence of the symmetry potential on the central density. This is done by comparing results obtained by using the MDI(0) with  $\text{MDYI}+U_{sym}^{MDI(0)}$ , and MDI(1) with  $\text{MDYI}+U_{sym}^{MDI(1)}$ , respectively. The two pairs of potentials correspond to the same symmetry energy of MDI(0) and MDI(1), respectively. It is seen that without the momentum-dependence of the symmetry potential, i.e.,  $\text{MDYI}+U_{sym}^{MDI(1)}$  and  $\text{MDYI}+U_{sym}^{MDI(0)}$  cases, the central density is slightly lower. This is because the symmetry potential is effectively stronger without the momentum-dependence as shown in Fig. 4. For neutron-rich matter this effectively stiffens the EOS, leading therefore to a lower compression. However, the general dynamics of the reaction is merely affected by the momentum-dependence of the symmetry potential.

## B. Effects on nucleon emissions

The generally repulsive/attractive symmetry potential for neutrons/protons at subnormal densities is to cause more neutrons/protons to be free/bound. We identify free nucleons

as those with local densities less than  $\rho_0/8$ . At midrapidity, the isospin asymmetry of free nucleons are dominated by the high-density behavior of nuclear symmetry energy. As the symmetry energy becomes more stiffer from the MDI(1) through MDI(0) to the  $E_{sym}^{RMF}(\rho)$  as shown in Fig. 2, gradually more/less neutrons/protons are expected to be emitted at midrapidity. The different symmetry energies will thus lead to quite different isospin asymmetries of free nucleons at mid-rapidity. Shown in the upper window of Fig. 7 are the nucleon rapidity distributions with the four different potentials. Since the three potentials MDI(1), MDI(0) and  $MDYI + U_{sym}^{RMF}(\rho)$  have about the same isoscalar part while their isovector parts are quite different, the observed difference among results using them clearly reveals the role of the symmetry potential in nucleon emissions. We also included the calculation with the  $SBKD + U_{sym}^{RMF}(\rho)$  interaction as a reference. First of all, it is seen that midrapidity nucleons are most sensitive to the variation of symmetry energy as one expects since these nucleons are the ones having gone through the high density phase. Moreover, neutron rapidity distributions are more affected by the symmetry energy than protons. The  $dN/dy$  values around midrapidity are higher for neutrons with the stiffer symmetry energies as one expects.



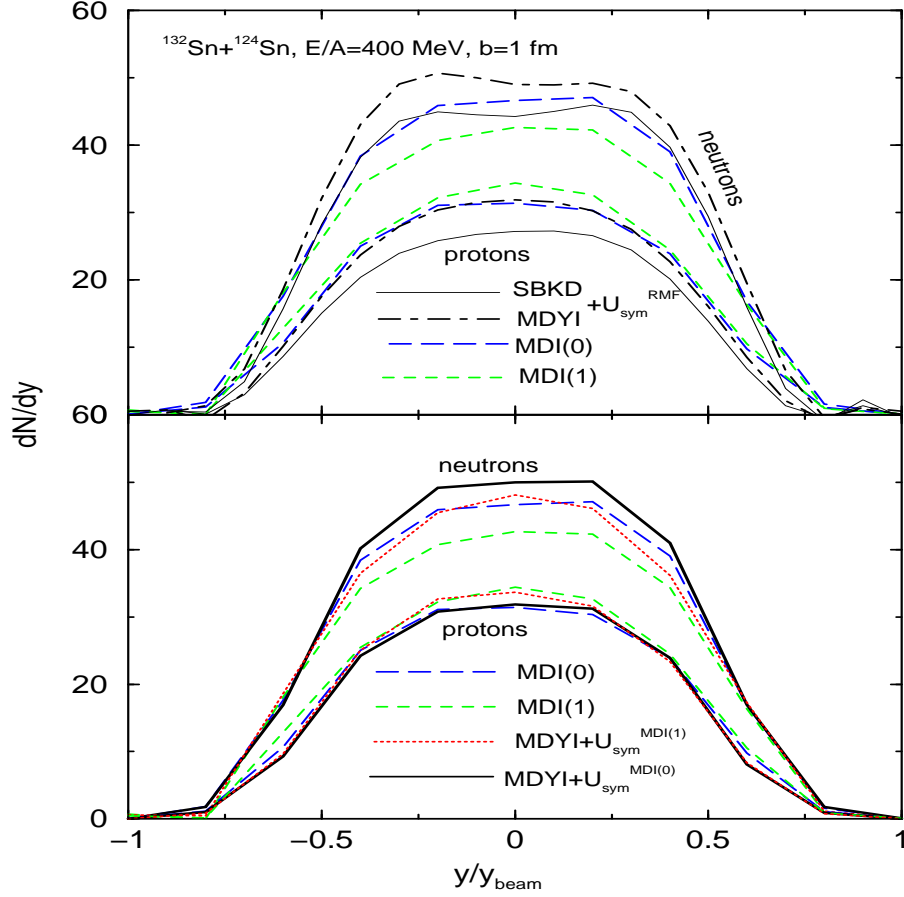


FIG. 7. Rapidity distributions of neutrons and protons with various potentials in the  $^{132}\text{Sn} + ^{124}\text{Sn}$  reaction at a beam energy of 400 MeV/nucleon and an impact parameter of 1 fm.

Included in the upper window Fig. 7 are also results obtained with the soft BKD isoscalar potential and the  $U_{sym}^{RMF}(\rho)$  symmetry potential. Compared to the calculations with the MDYI isoscalar potential but the same symmetry potential  $U_{sym}^{RMF}(\rho)$ , the soft BKD leads to reduced emissions of both neutrons and protons. In particular, the resulting neutron rapidity distribution is very close to the MDI(0) case. This illustrates one serious drawback of inclusive observables for studying the isospin-dependence of the nuclear EOS, such as the nucleon rapidity distributions studied here, that they are sensitive to both the isoscalar and isovector potentials. This is an important reason for us to concentrate on observables that

are only sensitive to the symmetry potential in the following sections.

What are the effects of the momentum-dependence of the symmetry potential on nucleon rapidity distributions? To answer this question we compare in the lower window of Fig. 7 nucleon rapidity distributions obtained with (MDI(0) and MDI(1)) and without ( $MDYI + U_{sym}^{MDI(0)}$  and  $MDYI + U_{sym}^{MDI(1)}$ ) the momentum-dependence in the symmetry potentials. It is seen that the momentum-dependence of the symmetry potential has very little effect on protons. This is mainly because the Coulomb potential works against and dominates over the symmetry potential on protons. However, the momentum-dependence of the symmetry potential affects significantly the neutron rapidity distributions. Overall, without the momentum-dependence of the symmetry potential (solid and dotted lines) the  $dN/Dy$  values for neutrons increases by 10 to 15% with respect to the results with the momentum-dependent symmetry potentials (long dashed and dashed lines). This increased emissions of neutrons are due to the stronger values of the symmetry potentials when the momentum-dependence is turned off as shown in Fig. 4.

### C. Effects on isospin fractionation

Isospin fractionation refers to the different isospin asymmetries in low and high density regions in nuclear reactions [34–36]. With symmetry energies increasing with density it is energetically more favorable to have the low density regions more neutron-rich while the high density regions more isospin symmetric. The strength of the isospin fractionation has been found to depend sensitively on the density-dependence of the symmetry energy [14,35,36]. As we have discussed in the previous subsection, the symmetry potential generally enhances the emission of neutrons while suppressing that of protons. A stiffer symmetry energy thus leads to a more neutron-rich low density gas of nucleons. Because of the charge and baryon number conservation, the remaining part (with local densities  $\rho \geq \rho_0/8$ ) is consequently more isospin symmetric. It should be noted that there is a net conversion of neutrons to protons because of the more abundant production of  $\pi^-$  than  $\pi^+$  above the pion production

threshold. This effect, however, is very small even at a beam energy of 2 GeV/nucleon [7].

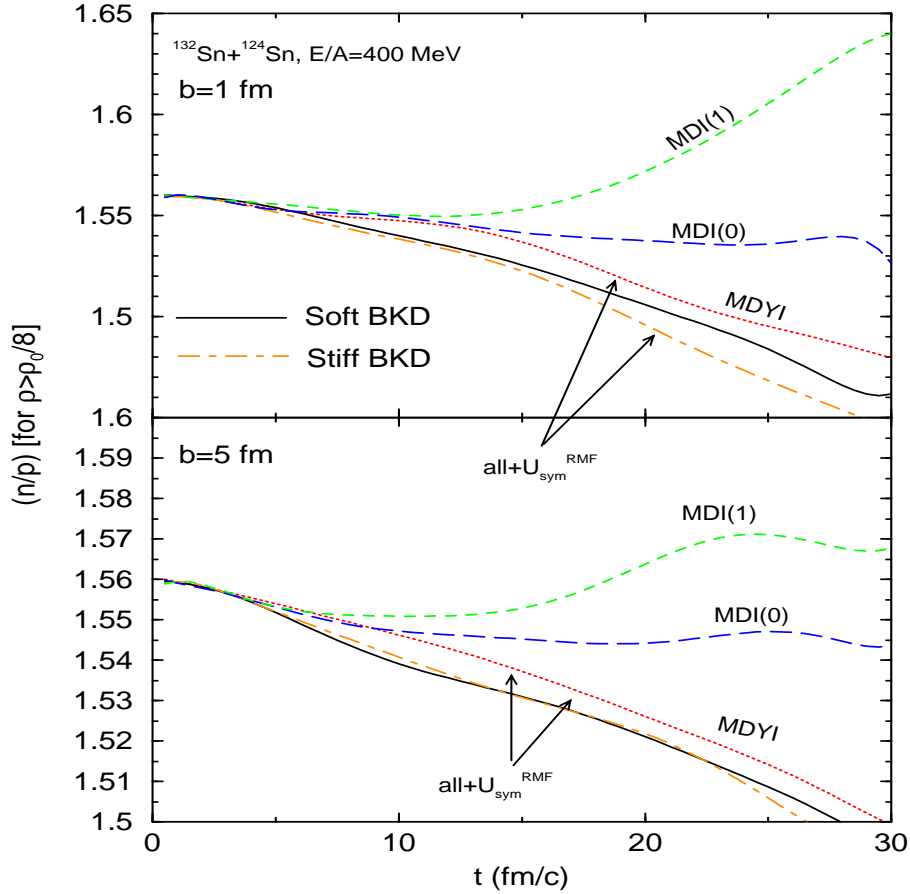


FIG. 8. Isospin asymmetry of bound nucleons in central (upper window) and midcentral (lower window) collisions of  $^{132}\text{Sn} + ^{124}\text{Sn}$  at a beam energy of 400 MeV/nucleon.

To first explore effects of the symmetry potential on isospin fractionation we study in Fig. 8 the isospin asymmetry (neutron/proton ratio) of bound nucleons as a function of time for central (upper window) and midcentral (lower window) collisions of  $^{132}\text{Sn} + ^{124}\text{Sn}$  at a beam energy of 400 MeV/nucleon. First of all, from the lowest three curves (the three calculations use three different isoscalar potentials but the same symmetry potential of  $U_{sym}^{RMF}$ ) in both windows, it is seen that the n/p ratio of bound nucleons (in the residue) is only slightly affected by the stiffness and the momentum-dependence of the isoscalar potential. They are calculated with the same symmetry potential  $U_{sym}^{RMF}(\rho)$  but three different isoscalar

potentials, the MDYI, soft BKD and the stiff BKD. There is only a variation of about 1-3% in the  $(n/p)_{\rho \geq \rho_0/8}$  ratio in the midcentral and central collisions. While it is very obvious that the  $(n/p)_{\rho \geq \rho_0/8}$  ratio is much more sensitive to the variation of the symmetry potential. It is seen that the isospin asymmetry of bound nucleons increases by about 12% and 5% in central and midcentral collisions, respectively, going from the stiffer to the softer symmetry energy (from the  $U_{sym}^{RMF}$  through MDI(0) to the MDI(1)).

What are the effects of the momentum-dependence of the symmetry potential on the isospin fractionation? We study this question in Fig. 9 by comparing results obtained with and without the momentum-dependence of the symmetry potential. It is interesting to see that although the momentum-dependence of the symmetry potential increases the overall magnitude of isospin asymmetry of bound nucleons, relative effects of the symmetry energy remain about the same. In fact, in central collisions with the momentum-dependence of the symmetry potential effects of the symmetry energy become even slightly stronger.

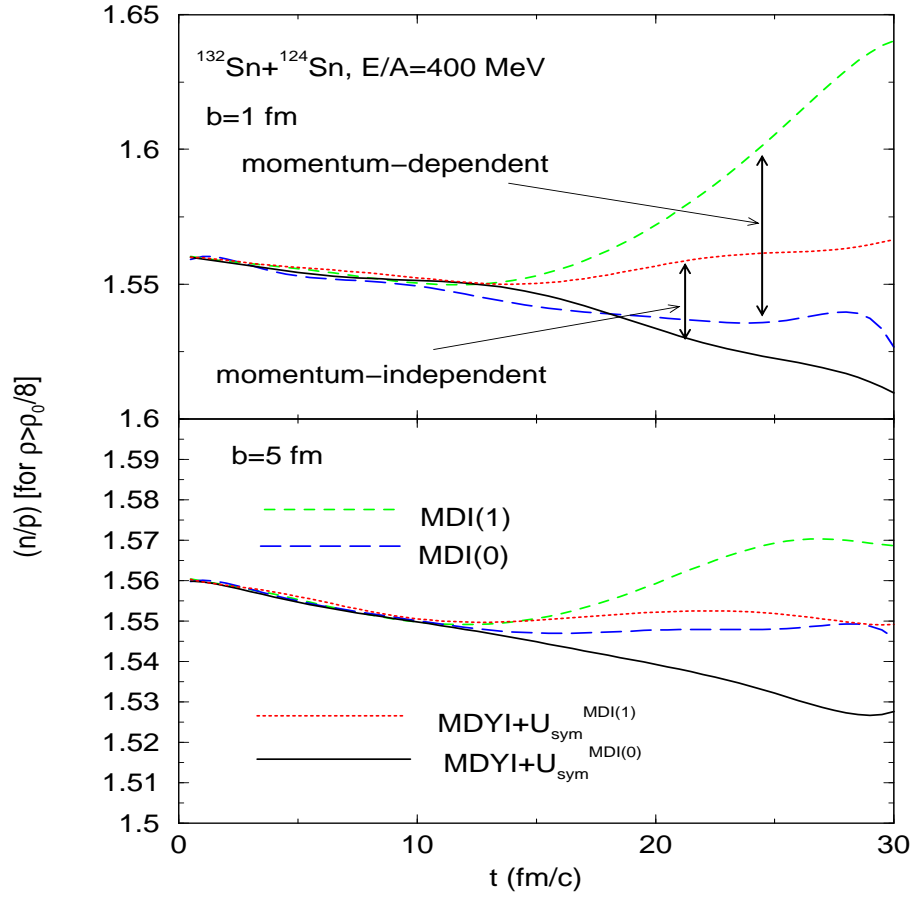


FIG. 9. Effects of the momentum-dependence of the symmetry potential on isospin asymmetry of bound nucleons in central (upper window) and midcentral (lower window) collisions of  $^{132}\text{Sn} + ^{124}\text{Sn}$  at a beam energy of 400 MeV/nucleon.

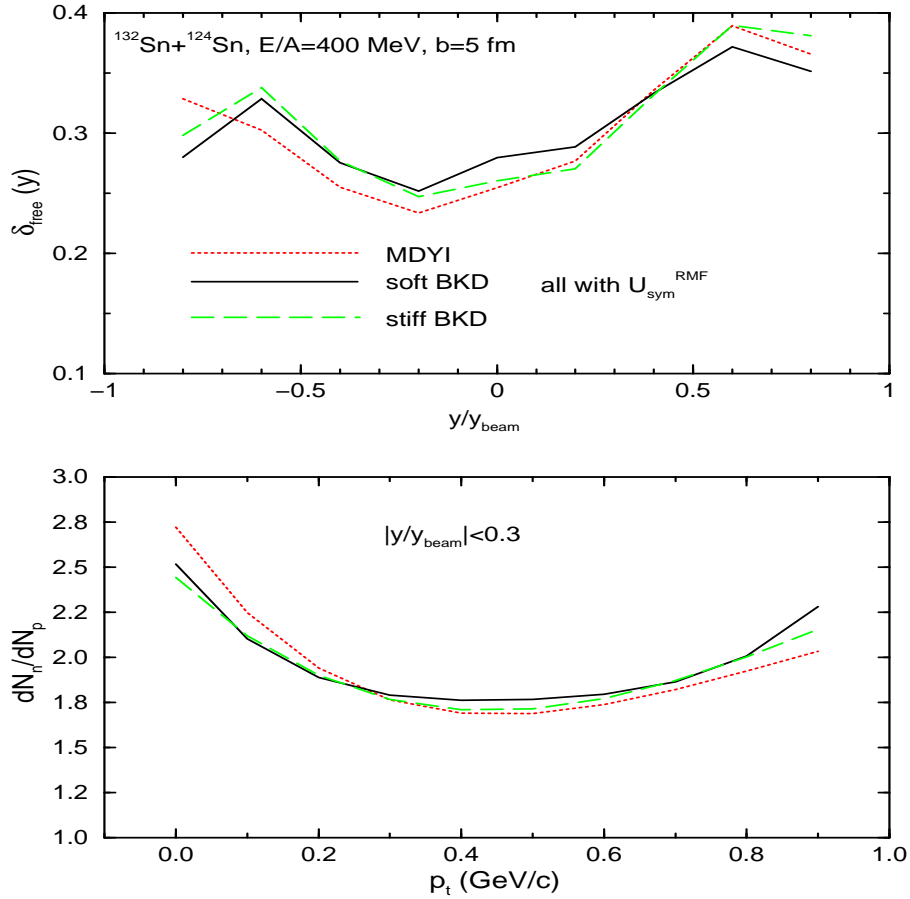


FIG. 10. Rapidity (upper window) and transverse momentum (lower window) distributions of isospin asymmetry of free nucleons with the three isoscalar potentials in the  $^{132}\text{Sn} + ^{124}\text{Sn}$  reaction at a beam energy of 400 MeV/nucleon and an impact parameter of 5 fm.

#### D. Combined constraints on density- and momentum-dependence of symmetry potentials

Since the  $n/p$  ratio of bound or free nucleons are mainly affected by the symmetry potential unlike the inclusive observables which are strongly affected by isoscalar potentials, we concentrate in this subsection on the isospin asymmetry of free nucleons. Our main focus is to find observables that can be combined together to constrain simultaneously both the density and the momentum dependence of the symmetry potential. Specifically, we study

the isospin asymmetry of free nucleons as a function of rapidity and transverse momentum. First, to show that these observables are indeed not so sensitive to the isoscalar potential we show in Fig. 10 the isospin asymmetry of free nucleons as a function of rapidity (upper window) and transverse momentum (lower window) calculated using the same symmetry potential  $U_{sym}^{RMF}(\rho)$  but the three different isoscalar potentials MDYI, soft BKD and stiff BKD. It is seen that there is a variation of less than 8% in the rapidity distribution of  $\delta_{free}$  by changing from the MDYI to the soft BKD. The n/p ratio of free nucleons at midrapidity is shown as a function of transverse momentum in the lower window. For this observable the variation due to the change in isoscalar potential is even smaller at all transverse momenta. It should be mentioned that the overall rise of  $dN_n/dN_p$  at low transverse momenta is due to the Coulomb repulsion on protons.

How can we constrain both the density- and momentum-dependence of the symmetry potential? Shown in the upper window of Fig. 11 are the isospin asymmetries of free nucleons calculated with and without the momentum-dependence of the symmetry potential as a function of rapidity. First of all, there is a shift downward when the momentum-dependence of the symmetry potential is included for both the soft (MDI(1)) and the stiffer (MDI(0)) symmetry energies. This is what we expected based on the comparisons of symmetry potentials in Fig. 4. Since the strength of the symmetry potential decreases with the increasing momentum, the reduction of  $\delta_{free}$  is particularly larger at higher rapidities. It is also interesting to note that effects of the density-dependence of the symmetry potential, particularly stronger at midrapidity, are about the same with or without the momentum-dependence of the symmetry potential. However, the value of  $\delta_{free}$  with the soft symmetry energy but without the momentum-dependence of the symmetry potential (dotted line) is about the same as the one obtained using the momentum-dependent stiff symmetry energy MDI(0) (long dashed) at midrapidity, although they are quite different at forward and backward rapidities.

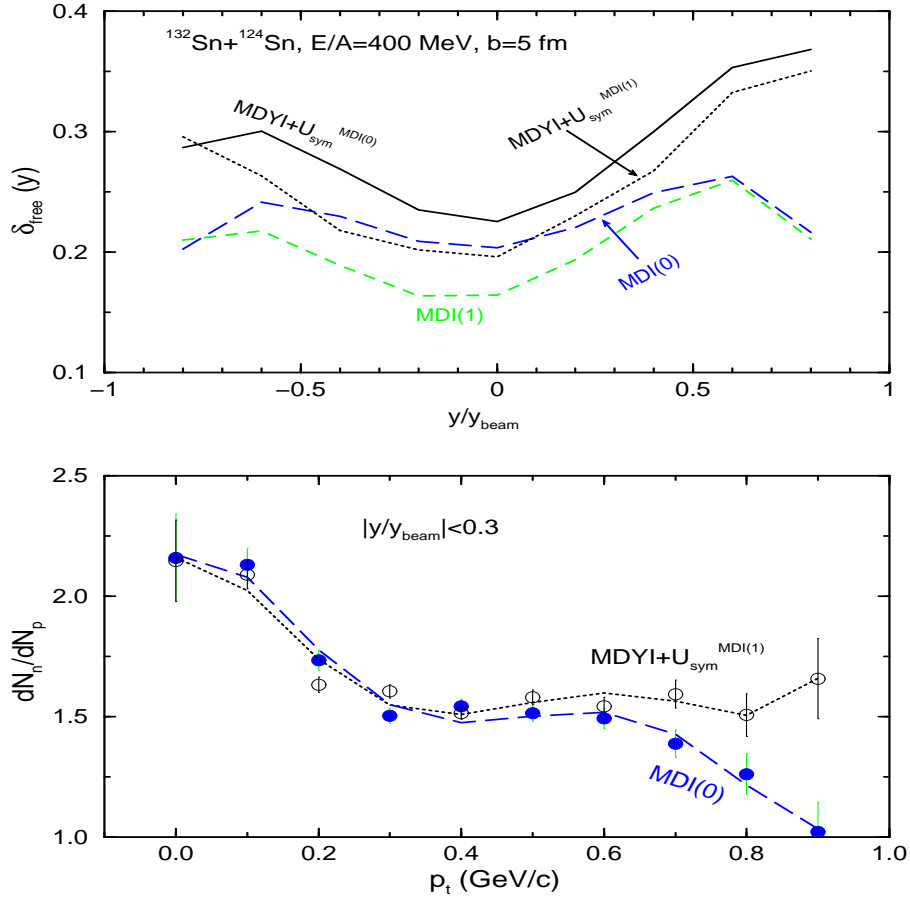


FIG. 11. Rapidity and transverse momentum distributions of isospin asymmetry of free nucleons with and without the momentum dependence of the symmetry potential in the  $^{132}\text{Sn} + ^{124}\text{Sn}$  reaction at a beam energy of 400 MeV/nucleon and an impact parameter of 5 fm.

How do we separate them at midrapidities? One possible way is shown in the lower window of Fig. 11 where we compare the ratio of free neutrons to protons at midrapidity as a function of transverse momentum with the  $\text{MDI}(0)$  and the  $\text{MDYI}+U_{sym}^{MDI(1)}(\rho)$  interactions. It is seen that the two interactions are clearly separated at high transverse momenta. This is mainly because the symmetry potential  $U_{sym}^{MDI(1)}(\rho)$  remains a constant while that embedded in the  $\text{MDI}(0)$  interaction decreases with increasing momenta as shown in Fig. 4. Thus by combining the measurements of the rapidity and transverse momentum distributions of the isospin asymmetry of free nucleons one can determine simultaneously the density-



and momentum-dependence of the symmetry potential. The density dependence of the symmetry energy can then be determined uniquely. We stress here that the separation at high transverse momenta is not due to the weaker isoscalar potential at high  $p_T$  with the MDI(0) interaction as shown in Fig. 5. This is because the isoscalar potential acts equally on both neutrons and protons, the ratio  $dN_n/dN_p$  is thus insensitive to the EOS of symmetric nuclear matter as shown in Fig. 10.

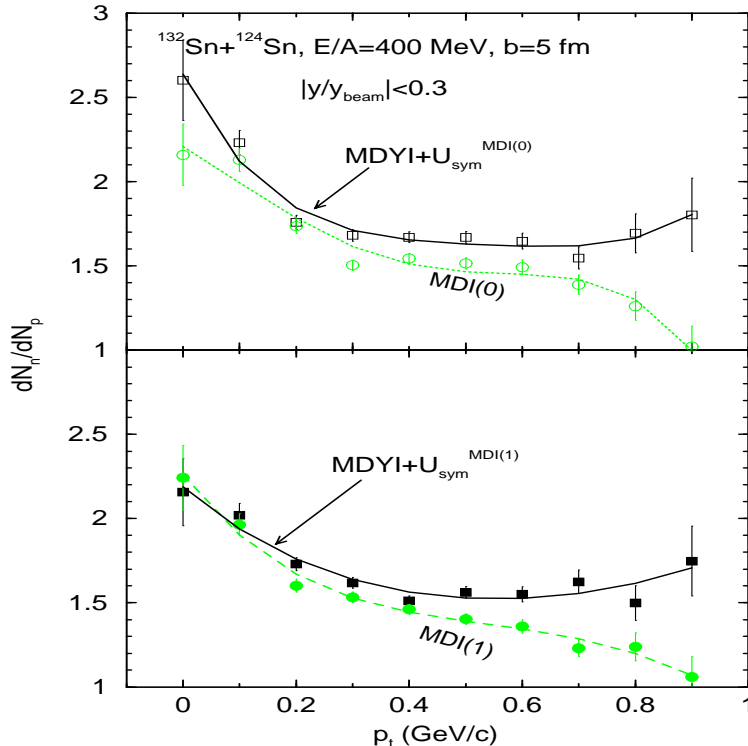


FIG. 12. Transverse momentum distributions of isospin asymmetry of free nucleons with and without the momentum dependence of the stiff (upper window) and soft (lower window) symmetry potential in the  $^{132}\text{Sn} + ^{124}\text{Sn}$  reaction at a beam energy of 400 MeV/nucleon and an impact parameter of 5 fm.

For a given density-dependent symmetry energy  $E_{\text{sym}}(\rho)$ , how does the momentum-dependence of the symmetry potential affect the  $p_t$  distribution of  $dN_n/dN_p$ ? To answer this question we compare in Fig. 12 the  $dN_n/dN_p$  distributions with the stiff (upper window)

and soft (lower window) symmetry energy with (open and filled circles) and without (open and filled squares) the momentum-dependence of the symmetry potential. It is seen that without the momentum-dependence of the symmetry potential, the  $dN_n/dN_p$  ratio turns to saturate above about  $p_t \geq 0.3\text{GeV}/c$ . With the momentum-dependence of the symmetry potential, however, the  $dN_n/dN_p$  continue to decrease to high  $p_t$  values. Again, this is a direct reflection of the decreasing symmetry potential with the increasing momentum. From both Fig. 11 and Fig. 12 one sees clearly the importance of measuring the isospin asymmetry of high  $p_t$  particles at midrapidity.

### **E. Effects on rapidity and transverse momentum dependence of free nucleons in central collisions**

In the previous subsection, we concentrated on midcentral collisions at an impact parameter of 5 fm. To examine the impact parameter dependence, we examine effects of the momentum-dependence of the symmetry potential in the  $^{132}\text{Sn} + ^{124}\text{Sn}$  reactions at 400 MeV/nucleon and an impact parameter of 1 fm with the soft and stiff symmetry energy in Fig. 13 and Fig. 14, respectively. Comparing the results at an impact parameter of  $b=1$  fm in Fig. 13 and Fig. 14 with those at an impact parameter of  $b=5$  fm in the previous subsection, it is seen that the main effects of the momentum-dependence of the symmetry potential do not change that much. This is mainly because for such a heavy reaction system as the  $^{132}\text{Sn} + ^{124}\text{Sn}$ , the variation of impact parameter from 1 fm to 5 fm does not result in a very appreciable change in both the density and the isospin asymmetry in the participant region during the reaction. More quantitatively, with the soft symmetry energy MDI(1) the effects of the momentum-dependence of the symmetry potential at  $b=1$  fm are somewhat stronger than that at  $b=5$  fm. However, with the stiff symmetry energy the impact parameter dependence is less obvious. This is understandable from the strength of the symmetry potentials shown in Fig. 4. It is seen there that the slope of the symmetry potential depends more strongly on the density in the case of the soft symmetry energy (MDI(1)). Thus, as the

density increases due to the increasing centrality, the force due to the symmetry potential increases more strongly with the soft symmetry energy, leading to the larger effects shown in Fig. 13.

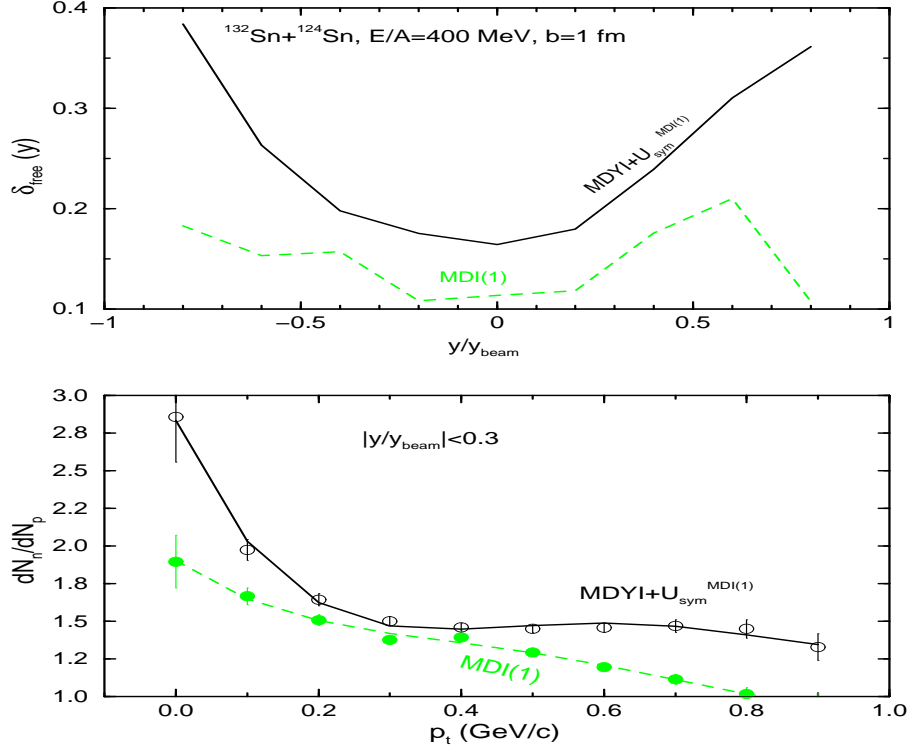


FIG. 13. Rapidity (upper window) and transverse momentum (lower window) distributions of isospin asymmetry of free nucleons with and without the momentum dependence of the *soft* symmetry energy in the  $^{132}\text{Sn} + ^{124}\text{Sn}$  reaction at a beam energy of 400 MeV/nucleon and an impact parameter of 1 fm.

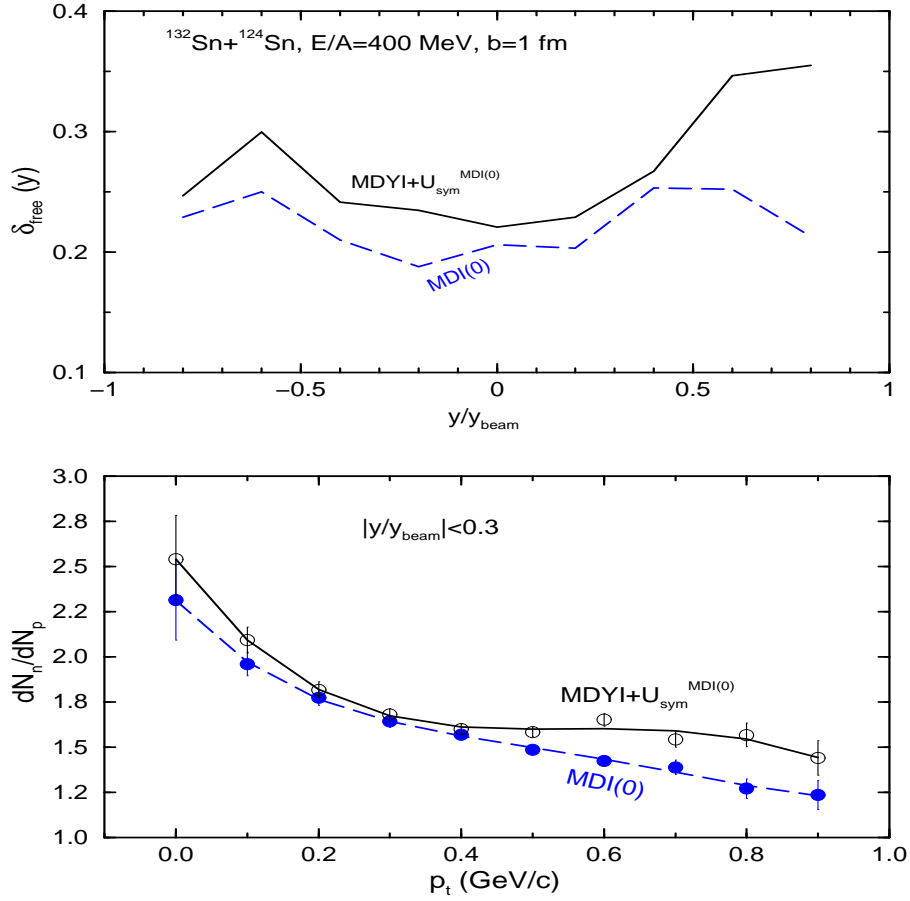


FIG. 14. Rapidity (upper window) and transverse momentum (lower window) distributions of isospin asymmetry of free nucleons with and without the momentum dependence of the *stiff* symmetry energy in the  $^{132}\text{Sn} + ^{124}\text{Sn}$  reaction at a beam energy of 400 MeV/nucleon and an impact parameter of 1 fm.

### F. Effects on proton direct flow and neutron-proton differential flow

How does the momentum-dependence of the symmetry potential affect the nuclear collective flow? First of all, it is important to know what collective observables are sensitive to the symmetry potential with or without the momentum-dependence. Since symmetry potential is small compared to the isoscalar potential, moreover, at high energies baryon-baryon collisions dominate the reaction dynamics, one has to use delicate observables to

extract information about the symmetry potential. To illustrate this point, we show in Fig. 15 the standard transverse flow analysis for protons in the reaction of  $^{132}\text{Sn} + ^{124}\text{Sn}$  at a beam energy of 400 MeV/nucleon and an impact parameter of 5 fm. It is seen that with (upper window) or without (lower window) the momentum-dependence of the symmetry potential for both the soft and stiff symmetry energies, the proton transverse flow is about the same.

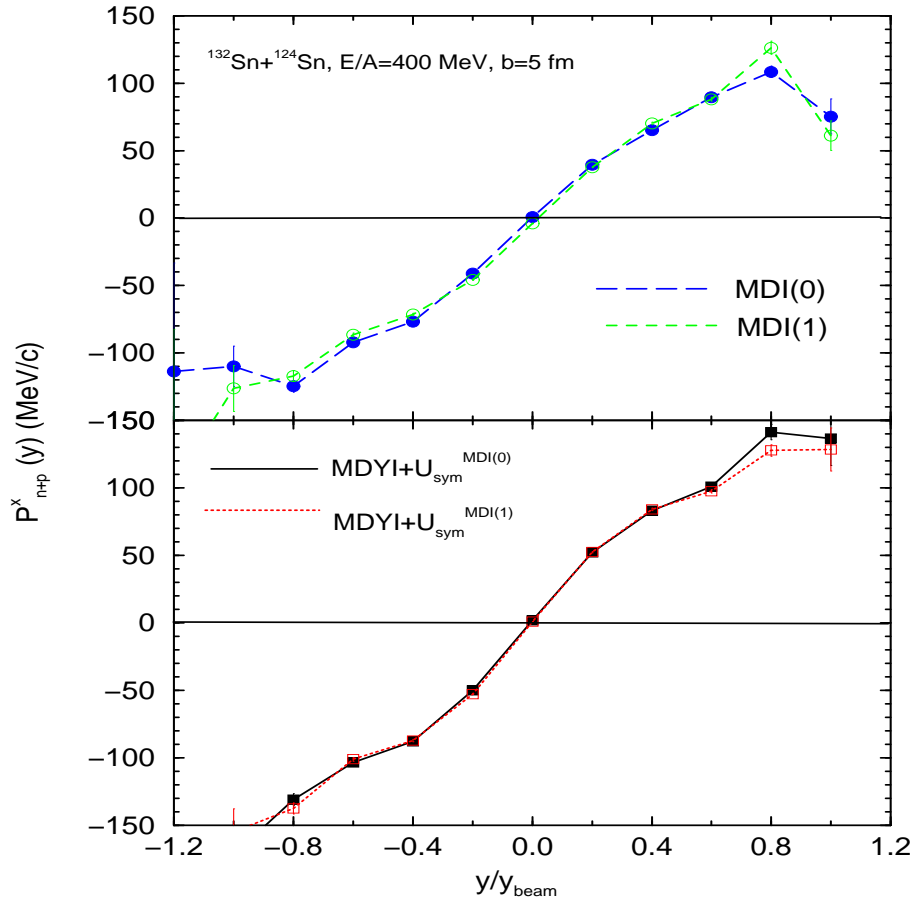


FIG. 15. Proton transverse flow analysis with (upper window) and without (lower window) the momentum-dependence of the symmetry potential in the reaction of  $^{132}\text{Sn} + ^{124}\text{Sn}$  at a beam energy of 400 MeV/nucleon and an impact parameter of 5 fm.

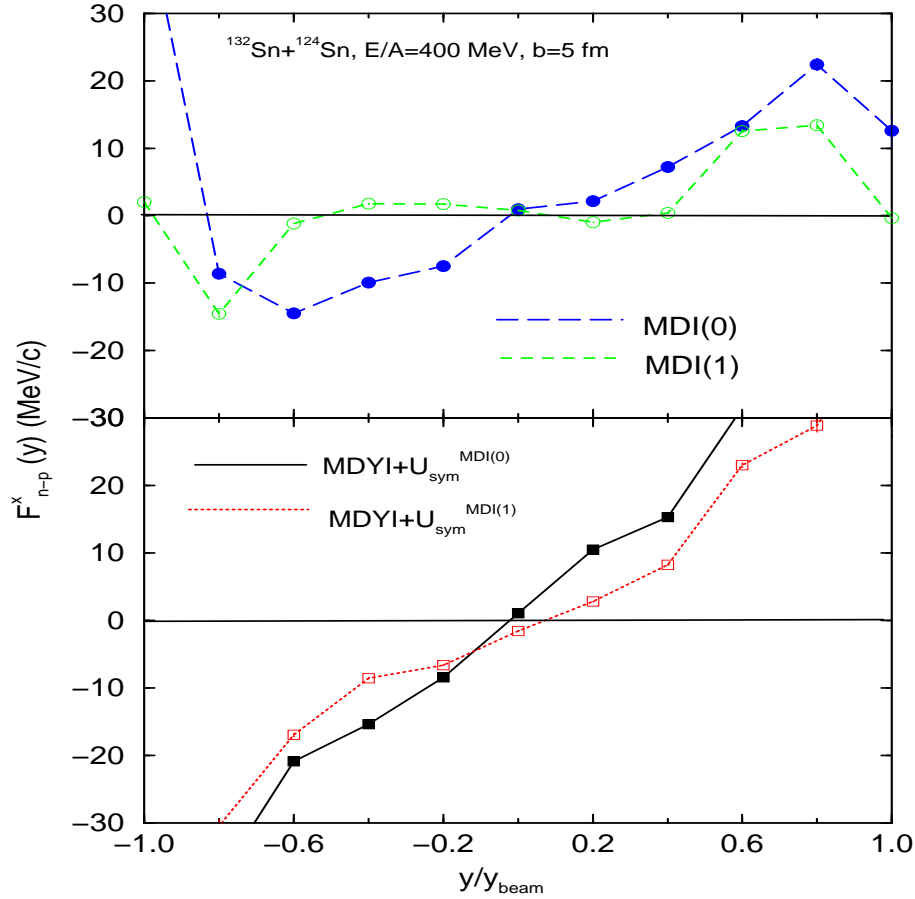


FIG. 16. Neutron-proton differential flow analysis with (upper window) and without (lower window) the momentum-dependence of the symmetry potential in the reaction of  $^{132}\text{Sn} + ^{124}\text{Sn}$  at a beam energy of 400 MeV/nucleon and an impact parameter of 5 fm.

We now turn to the neutron-proton differential flow

$$F_{n-p}^x(y) \equiv \sum_{i=1}^{N(y)} (p_i^x w_i) / N(y), \quad (16)$$

where  $w_i = 1(-1)$  for neutrons (protons) and  $N(y)$  is the total number of free nucleons at rapidity  $y$ . The differential flow combines constructively effects of the symmetry potential on the isospin fractionation and the collective flow. It has the advantage of maximizing effects of the symmetry potential while minimizing effects of the isoscalar potential [14]. Shown in Fig. 16 is the neutron-proton differential flow with (upper window) and without (lower window) the momentum-dependence of the symmetry potential. First, it is seen that in both cases,

the neutron-proton differential flow is rather sensitive to the symmetry energy compared to the standard proton transverse flow analysis shown in Fig. 15. Secondly, it is seen that the neutron-proton differential flow is stronger without the momentum-dependence of the symmetry potential. This is because the momentum-independent symmetry potential makes not only more neutrons free but also gives them higher transverse momenta in the reaction plane because of its higher magnitude and steeper slopes compared to the momentum-dependent symmetry potential embedded in eq. 2.

Is the neutron-proton differential flow still sensitive to the variation of  $E_{sym}(\rho)$  when the momentum-dependent symmetry potential is used? The answer is a definitely yes as shown in the upper window of Fig. 16. In fact, the slope of the differential flow  $F_{n-p}^x(y)$  at  $y=0$  changes from about -1.9 to 21.4 MeV/c using eq. 2 by changing from the MDI(1) to the MDI(0) parameter set, while it changes from about 26 to 39 MeV/c with the momentum-independent symmetry potentials. The net change due to the variation of the  $E_{sym}(\rho)$  is thus actually larger with the momentum-dependent symmetry potentials. Thus the neutron-proton differential flow remains a sensitive probe to the density dependence of the symmetry energy.

#### IV. SUMMARY

In summary, using an isospin- and momentum-dependent transport model we studied effects of the momentum-dependent symmetry potential on several experimental observables in heavy-ion collisions induced by neutron-rich nuclei at RIA energies. The momentum-dependence of the symmetry potential is found to play an important role in the isospin fractionation, particle emission and neutron-proton differential flow. In particular, high  $p_t$  neutron to proton ratio at midrapidity is very sensitive to the momentum-dependence of the symmetry potential. However, the momentum-dependence of the symmetry potential has little effects on the overall reaction dynamics and the directed nuclear flow. To uniquely determine the  $E_{sym}(\rho)$  one needs to determine simultaneously both the density-

and momentum-dependence of the symmetry potential. For this purpose, it is necessary to combine several experimental observables, such as, the rapidity and transverse momentum dependence of the free neutron to proton ratio, and the neutron-proton differential flow. Comparing experimental data with predictions based on transport models including the momentum-dependent symmetry potential is thus crucial for investigating accurately the EOS of dense neutron-rich matter.

## V. ACKNOWLEDGEMENT

This research is supported in part by the National Science Foundation of the United States under grant No. PHY-0088934, PHY-0243571, the Natural Sciences and Engineering Research Council of Canada, and the Fonds Nature et Technologies of Quebec.



## REFERENCES

- [1] H.A. Bethe, Rev. Mod. Phys. **62**, 801 (1990).
- [2] J.M. Lattimer and M. Prakash, Astr. Phys. Jour. **550**, 426 (2001).
- [3] *Isospin Physics in Heavy-Ion Collisions at Intermediate Energies*, Eds. B. A. Li and W. Udo Schröder (Nova Science Publishers, Inc, New York, 2001).
- [4] I. Bombaci, in ref. [3], p.35.
- [5] B.A. Li, C.M. Ko, and W. Bauer, topical review, Int. Jour. Mod. Phys. E **7**, 147 (1998).
- [6] P. Danielewicz, R. Lacey and W.G. Lynch, Science 298, 1592 (2002).
- [7] B.A. Li, Phys. Rev. Lett. 88, 192701 (2002); Nucl. Phys. A**708**, 365 (2003).
- [8] The DOE/NSF Nuclear Science Advisory Committee, Opportunities in Nuclear Science, April (2002).
- [9] B.A. Li, C.M. Ko, and Z.Z. Ren, Phys. Rev. Lett. **78**, 1644 (1997).
- [10] M.B. Tsang et al., Phys. Rev. Lett. **86**, 5023 (2001).
- [11] W.P. Tan *et al.*, Phys. Rev. C **64**, 051901(R) (2001).
- [12] V. Baran, M. Colonna, M. Di Toro, V. Greco, M. Zielinska-Pfabé and H.H. Wolter, Nucl. Phys. A **703**, 603 (2002).
- [13] M.B. Tsang et al., Phys. Rev. Lett. (2004) in press, nucl-ex/0310024.
- [14] B.A. Li, Phys. Rev. Lett. **85**, 4221 (2000).
- [15] V. Greco, M. Colonna, M. Di Toro and F. Matera, Phys. Rev. C**67**, 015203 (2003).
- [16] L. Scalone, M. Colonna and M. Di Toro, Phys. Lett. **B461**, 9 (1999).
- [17] L.W. Chen, V. Greco, C.M. Ko and B.A. Li, Phys. Rev. Lett. **90**, 162701 (2003); Phys. Rev. C**68**, 014605 (2003).

- [18] L.W. Chen, C.M. Ko and B.A. Li, Phys. Rev. **C68**, 017601 (2003); Nucl. Phys. **A729**, 809 (2003).
- [19] J. Rizzo, M. Colonna, M. Di Toro and V. Greco, Nucl. Phys. **A732** (2004) 202.
- [20] C. Gale, G. Bertsch and S. Das Gupta, Phys. Rev. **C35**, 1666 (1987).
- [21] M. Prakash, T.T. S. Kuo and S. Das Gupta, Phys. Rev. **C37**, 2253 (1988); G.M. Welke, M. Prakash, T.T. S. Kuo and S. Das Gupta, *ibid* **C38**, 2101 (1988).
- [22] C. Gale et al., Phys. Rev. **C41**, 1545 (1990).
- [23] V. Koch et al., Phys. Lett. **B206**, 395 (1988); Nucl. Phys. **A532**, 715 (1991); B. Blaettel, V. Koch and U. Mosel, Rep. Prog. Phys., 56, 1 (1993).
- [24] P. Danielewicz and G.F. Bertsch, Nucl. Phys. **A533**, 712 (1991); Q. Pan and P. Danielewicz, Phys. Rev. Lett. **70**, 2062 (1993); P. Danielewicz, Nucl. Phys. **A673**, 375 (2000).
- [25] L.P. Csernai, G. Fai, C. Gale and E. Osnes, Phys. Rev. **C46**, 736 (1992); V.K. Mishra, G. Fai, L.P. Csernai and E. Osnes, *ibid*, **C47**, 1519 (1993).
- [26] J. Zhang, S. Das Gupta and C. Gale, Phys. Rev. **C50**, 1617 (1994).
- [27] C.B. Das, S. Das Gupta, C. Gale and B.A. Li, Phys. Rev. **C67**, 034611 (2003).
- [28] B.A. Li, C.B. Das, S. Das Gupta and C. Gale, Phys. Rev. **C69**, 011603 (2004).
- [29] P.E. Hodgson, The Nucleon Optical Model, 1994 (World Scientific).
- [30] R.B. Wiringa, Phys. Rev. **C38**, 2967 (1988).
- [31] G.F. Bertsch, H. Kruse and S. Das Gupta, Phys. Rev. **C29**, 673 (1984).
- [32] B.A. Brown, Phys. Rev. Lett. **85**, 5296 (2000).
- [33] R.B. Wiringa et al., Phys. Rev. **C38**, 1010 (1988).

- [34] H. Müller and B.D. Serot, Phys. Rev. C**52**, 2072 (1995).
- [35] B.A. Li and C.M. Ko, Nucl. Phys. **A618**, 498 (1997).
- [36] V. Baran, A. Larionov, M. Colonna and M. Di Toro, Nucl. Phys. **A632**, 287 (1998).
- [37] I. Bombaci and U. Lombardo, Phys. Rev. C**44**, 1892 (1991).